Aerodynamic Shape Optimization of a Gas Turbine Engine Air-Delivery Duct

Krzysztof Marchlewski[1]; Łukasz Łaniewski-Wołłk, Ph.D.[2]; and Sławomir Kubacki, Ph.D.[3]

Abstract: We discuss a methodology for multiobjective optimization of the U-shaped air-delivery duct, which is a part of a turboprop engine intake system. The methodology combines and extends existing techniques to optimize the real-world engineering problem efficiently. The procedure utilizes Kriging models for the approximation of objective functions. We use the Expected Hypervolume Improvement method for improving the Kriging models accuracy and creating the Pareto front. The calculations are parallel and asynchronous, allowing to reduce the time needed for finding the optimal designs. The algorithm is resistant to solver failures and mesh issues. We perform the optimization with a purpose to satisfy two objectives: reduction of a total pressure loss across the duct and improvement/not-worsening of a distortion coefficient at the duct outlet. To obtain the improvement, we modify the shape of the duct within limits to fulfill geometric constraints. We use 30 design variables to control the deformation of the duct surface based on radial basis function interpolation. **DOI: 10.1061/(ASCE)AS.1943-5525.0001157.**

Author keywords: Multiobjective optimization; Kriging model; Expected hypervolume improvement; Parallelization; U-shaped duct.

Introduction

Growth in a value of a power-to-weight ratio of modern aeroengines and availability of low-price jet fuel motivates the aircraft industry to replace piston engines by turboprop engines in air transport services provided by small aircraft. Since the development of new turboprop engines is a very complex process, it becomes apparent that some small aircraft are currently built on existing engines. As the result of a change of the propulsion unit from the piston engine to the turboprop engine, an adjustment of selected I-23 airframe components was undertaken in the frame of the European Union project "Efficient Systems and Propulsion for Small Aircraft"—ESPOSA. The baseline air-delivery duct was designed at the Institute of Aviation in Warsaw, Poland (Stalewski and Żółtak 2014). The initial design suffered from a small flow separation at the duct outlet. This flaw was removed by Soemarwoto et al. (2016), who conducted the shape optimization of the duct. In the study, a deviation from a desirable pressure distribution was chosen as the objective function. A function gradient, calculated using the adjoint method, was used to find an optimal duct shape. The present work is intended to improve further the duct shape obtained by Soemarwoto et al.

We begin with the examples of the air-delivery ducts optimizations. It allows the reader to determine a relation between our method and existing ones. The choice of the optimization technique is heavily dependent on available computational resources, which limits the accuracy of flow simulations and a number of optimization variables controlling the duct shape. Another noteworthy factor is the number of objective functions. With more than one objective function, one has to prepare a Pareto front to facilitate a choice of an adequate design. Clearly, it increases the computational cost of the optimization process.

Let us start with examples of the optimization processes that do not use any modeling technique to approximate objective function. Aranake et al. (2011) performed the multiobjective optimization of an S-shaped duct employing two geometrical variables. The flow simulations were relatively fast and took 2 h each. The small number of variables and the low simulation cost allowed authors to take advantage of the multiobjective genetic algorithm to create the Pareto front. Comparable multiobjective shape optimization strategies were considered by Furlan et al. (2014) and Chiereghin et al. (2017). Both studies differ in some aspects, such as the number of geometrical variables controlling the geometry, but a common feature was to limit the complexity of the flow simulation methods to obtain acceptable optimization times. D'Ambros et al. (2018) applied the approach based on a Tabu search algorithm. The authors performed the multiobjective optimization of an S-shaped duct. They applied a free-form deformation approach with 36° of freedom. A substantial improvement in the values of both objective functions was reported, but 1,300 simulations were needed to obtain the results. The authors also noted that the additional simulations would be needed to create a more accurate Pareto front.

We already mentioned the work by Soemarwoto et al. (2016), who conducted the gradient-based optimization of the U-shaped duct using the adjoint method. This approach is frequently applied because it allows calculating the gradient of the objective function at a low cost. A disadvantage of this method is limited availability of the adjoint solvers. A comparable optimization was performed by Alessi et al. (2019). The U-shaped channel, which is a part of an internal cooling system of the gas turbine, was optimized. The adjoint method was implemented in the OpenFOAM

[1]Warsaw Univ. of Technology, Faculty of Power and Aeronautical Engineering, Institute of Aeronautics and Applied Mechanics, Nowowiejska 24, 00-665 Warsaw, Poland (corresponding author). ORCID: https://orcid.org/0000-0003-0751-9035. Email: kmarchlewski@meil.pw.edu.pl

[2]Warsaw Univ. of Technology, Faculty of Power and Aeronautical Engineering, Institute of Aeronautics and Applied Mechanics, Nowowiejska 24, 00-665 Warsaw, Poland. ORCID: https://orcid.org/0000-0002-3026-5881. Email: llaniewski@meil.pw.edu.pl

[3]Warsaw Univ. of Technology, Faculty of Power and Aeronautical Engineering, Institute of Aeronautics and Applied Mechanics, Nowowiejska 24, 00-665 Warsaw, Poland. Email: slawomir.kubacki@pw.edu.pl

Note. This manuscript was submitted on June 18, 2019; approved on February 24, 2020; published online on May 13, 2020. Discussion period open until October 13, 2020; separate discussions must be submitted for individual papers. This paper is part of the ***Journal of Aerospace Engineering***, © ASCE, ISSN 0893-1321.

version 3.0+ open-source framework. The authors reported a 30% reduction of the pressure loss in comparison with the base design.

Now, let us proceed with the examples of the optimization processes that take advantage of the response surface models. These models are also called metamodels and surrogate models. They are commonly applied to optimize the expensive black-box functions efficiently. The most popular models include artificial neural networks, radial basis functions, splines, and Kriging. They allow one to prepare an approximation of the objective function utilizing a certain number of its evaluations. Most of such techniques have two basic steps in common. In the beginning, a Design of Experiments is performed. It involves choosing preliminary designs for which the objective function is evaluated. The obtained values are used to create the metamodel. Further steps may be chosen in different ways. The simplest and least accurate approach consists in finding an optimum point of the model. It is important that the calculation of the model response is much cheaper than the evaluation of the objective function. It makes the search for the optimum fast. Such an approach was used by Namgoong et al. (2008), who conducted the shape optimization of a U-shaped channel to obtain minimal pressure loss. The authors used a genetic algorithm to find the minimum point of the Kriging model and chose it as an optimal design. A much more effective technique is to enlarge the initial set of designs with the obtained point, and to calculate the corresponding objective function value and create a new model. By doing this iteratively, one can obtain a better estimation of the optimum point. However, this approach may lead us to the local optimum. Zerbinati et al. (2012) performed the multiobjective optimization of a U-shaped duct. The pressure loss across the duct and the velocity variance at the duct outlet were chosen as the objectives. In each iteration, the authors used a generalization of the steepest-descent method to find a nondominated set of designs using the actual Kriging models. Then, they calculated the corresponding objective functions values and created the new models. The procedure was repeated nine times, which resulted in finding a design for which a 36% improvement of the pressure loss was obtained and a design for which the velocity variance was decreased by 37%. A study by Verstraete et al. (2013) describes the shape optimization of the U-bended cooling channel in order to reduce the pressure loss. The approach is almost the same as in the previous article, but this time a differential evolutionary algorithm (Storn and Price 1997) was used to find a metamodel minimum. Two types of models were tested: a Kriging model and an artificial neural network model. The optimization based on the Kriging model allowed authors to obtain slightly better results—a 37.6% reduction of the pressure loss. Verstraete and Li (2013) used the same methodology to optimize the same channel but in the presence of two objective functions, the pressure loss and the heat flow rate. They reported a decrease in the pressure loss by 12% ∼ 30% and an increase in the heat flow rate by 8% ∼ 17%. Gan and Zhang (2017) also conducted the multiobjective optimization of the S-shaped duct. The authors selected the flow distortion coefficient and the total pressure recovery as the objective functions. To prepare the approximations, they chose models based on the radial basis functions. The multiobjective genetic algorithm allowed the group to find the optimal design characterized by the distortion coefficient reduced by 16.3% and the total pressure recovery factor increased by 1.1%. A work by Raghavan and Breitkopf (2013) describes the multiobjective optimization of the S-shaped duct, but the usage of the metamodel is different from the previous studies. The group put the emphasis on the parallelism and the asynchronicity of the objective functions calculations. To perform the optimization, the genetic algorithm was chosen due to its good scalability. Nevertheless, in such cases, the algorithm has to wait with a generation of the new population until all calculations within the previous population are completed. Raghavan and Breitkopf proposed that in such cases the prediction of the metamodel can be used to substitute for missing results and proceed with the optimization process.

As we mentioned, the optimization methods that utilize the optima of the consecutively updated metamodels have a tendency to find the local optimum of the objective function instead of the global one. This inconvenient feature is almost absent in the approach proposed by Jones et al. (1998). It consists of the usage of the Kriging model and the Expected Improvement function and gives rise to the Efficient Global Optimization method (Jones et al. 1998). The Expected Improvement function allows one to balance the local and global search for the minimum point. The function is a measure that provides information on what are the chances of improving the actual minimum if the evaluation of the objective function is going to be performed in a selected point. Bae et al. (2012) used exactly that approach for S-shaped duct optimization. Girdziusas et al. (2012) also applied the Efficient Global Optimization method and conducted the duct optimization. They used a multipoint variant of the Expected Improvement method (Schonlau 1997) and performed four evaluations of the objective function simultaneously. Kriging models are used in an interesting way in a work by Venturelli and Benini (2016). The group optimized an S-shaped duct in the presence of two objective functions. To do so, they utilized a special genetic algorithm that is enhanced by the Kriging models. Finally, the authors use these models for a better selection of offspring.

The present work discusses the methodology for the multiobjective optimization of air-delivery duct shape. The novelty of our approach consists of combining existing techniques and methodologies into a complete procedure allowing the optimization of a real-life problem. We chose the elements of the procedure to make the optimization process easy in application and feasible in industrial conditions. In particular, such conditions mean treating the solver as the black-box, which is vulnerable to problems with the solver convergence, mesh quality, and numerical resources.

The goals of the optimization are the reduction of the total pressure loss across the duct and the improvement/not-worsening of the flow distortion coefficient at the duct outlet. We employ a method of the optimization based on the Kriging model (Krige 1951; Roustant et al. 2012; Shahriari et al. 2015). To handle two objective functions, we employ the Expected Hypervolume Improvement (EHVI) method (Bradstreet 2011; Łaniewski-Wołłk 2010), which allows us to create a Pareto front. For industrial applications, it is important that the optimization process is relatively fast and resistant to solver/mesh issues and varying availability of computational resources. We ensure this by modifying the Efficient Global Optimization method to be parallel and asynchronous. It means that there is no necessity for the optimization process to wait for an ongoing evaluation to finish to proceed with the optimization. The unavailable objective function value is estimated with the Kriging model. Then, this estimation is used to create a new model. This technique can be repeated a few times to obtain a necessary number of parallel objective function calculations. The approach is sometimes called the Kriging believer heuristic [see e.g., (Ginsbourger et al. 2010)]. Detailed information on the method is provided in the following paragraphs.

Computational Setup

The U-duct, which is the subject of the optimization process, is the main part of the turboprop engine air-delivery system. The first design was prepared by Stalewski and Żółtak (2014) and subsequently

improved by Soemarwoto et al. (2016), who conducted the shape optimization in order to obtain better flow characteristics. We treat the result obtained by Soemarwoto et al. (2016) as our baseline design and improve it further. To do so, we chose two objective functions: the total pressure loss across the duct and the flow uniformity at the duct outlet. The pressure loss is minimized, and the uniformity is maximized.

Flow Conditions and Objective Functions

Fig. 1 shows the fluid part of the air-intake duct and dummy volume serving as a simplified compressor. The circular surface called *fan* is defined inside the dummy volume to impose the pressure gradient there. This pressure gradient drives the flow through the duct. The aerodynamic interface plane (AIP) is constructed at the duct outlet (entrance to the compressor) to calculate the total pressure there. The bar behind the duct denotes the closest element of the engine mounting system. This element serves as a geometric constraint in the current optimization process.

The constant value of the pressure jump Δp is imposed across the fan surface. This pressure difference is estimated from the Bernoulli equation for the cruise flight at high altitude (3,000 m above ground) in order to satisfy the required mass flow rate $\dot{m} = 1.333$ kg/s through the A_{AIP}: surface

$$\Delta p = \frac{\rho \cdot (U_2^2 - U_{\text{inf}}^2)}{2} = 7265[\text{Pa}] \tag{1}$$

where $\rho = 0.91$ kg/m^3, $U_{\text{inf}} = 71$ m/s, $U_2 = \dot{m}/\rho A_{\text{AIP}}$, and $A_{\text{AIP}} = 0.01$ m^2.

Notice that the precise characteristics of the compressor are not available from a manufacturer. The Reynolds number based on the hydraulic diameter and the velocity at the inlet to the duct is equal to $\text{Re} = 3.8 \times 10^5$. The flow is treated as fully turbulent.

We use two objective functions: the pressure loss Δp_{l} and the distortion coefficient DC_{60}, which is the measure of the flow uniformity (for a uniform flow $\text{DC}_{60} = 0$). These are defined as

$$\Delta p_{\text{l}} = p_t^{\text{inlet}} - p_t^{\text{AIP}} \tag{2}$$

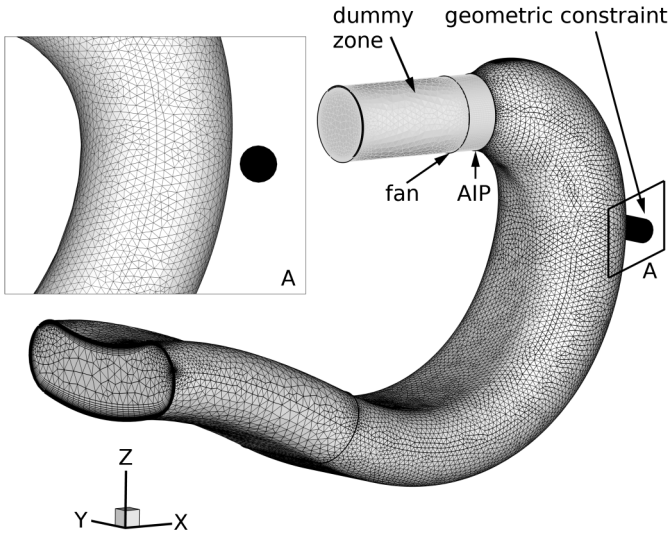

Fig. 1. View of computational mesh on duct surface and air inlet/outlet boundaries. Bar behind duct is closest element of engine mounting system, which serves as geometric constraint.

$$\text{DC}_{60} = \frac{p_t^{\text{AIP}} - p_{t,60}^{\text{AIP}}}{p_d^{\text{AIP}}} \tag{3}$$

where p_t^{inlet} = area-averaged total pressure at inlet to the duct; p_t^{AIP} = area-averaged total pressure on the AIP; $p_{t,60}^{\text{AIP}}$ = area-averaged total pressure computed on the 60°-sector of the AIP face for which the minimum area-averaged total pressure is achieved; and p_d^{AIP} = area-averaged dynamic pressure on the AIP.

The definition of $p_{t,60}^{\text{AIP}}$ is as follows:

$$p_{t,60}^{\text{AIP}} = \min_{\substack{\theta = \frac{k\pi}{3}, \\ k = 0, \ldots 5}} p_t^{\text{AIP}}\left(\theta - \frac{\pi}{6}, \theta + \frac{\pi}{6}\right) \tag{4}$$

Flow Simulation

We performed the computational fluid dynamics (CFD) simulations with the ANSYS Fluent solver version 14.0. We treated the flow as compressible. The convective terms in all equations are discretized with the second-order upwind scheme. The continuity, momentum, and energy equations are solved as a coupled system of equations (density-based solver of ANSYS Fluent) with Courant-Friedrichs-Lewy (CFL) number set to 5. The transport equations for the turbulent model are solved sequentially. We assumed that the solution is satisfactory when the normalized residuals for the mass, momentum, energy equations, and the scalar transport equations for the k-ω SST turbulence model are lower than 10^{-5}.

The computational mesh that we constructed is a hybrid mesh. It consists of the boundary layer mesh near the duct surface and the unstructured mesh elements in the interior of the duct. The total number of cells for both the duct and the dummy zone is equal to 1.7 million. The value of y^+ parameter is less than 3 (Fig. 2) over most of the duct surface (for more than 90% of the surface). Somewhat higher values are reported near the inlet to the dummy volume ($y^+ = 8$). The grid quality inside the dummy zone is irrelevant for the present study. The enhanced wall-function technique is employed at all surfaces of the duct for simulation with the k-ω SST model, with the curvature correction term active (Smirnov and Menter 2009).

Validation of the Turbulence Model

In this section, a validation of the standard k-ϵ model (with and without the curvature-correction term) and the k-ω SST model

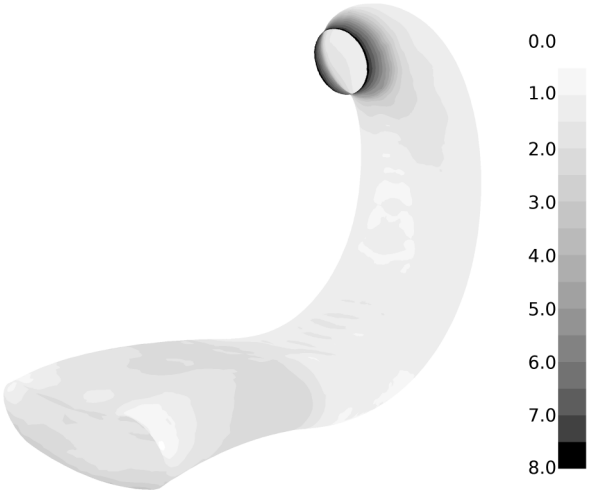

Fig. 2. Values of y^+ parameters plotted on air-duct surface.

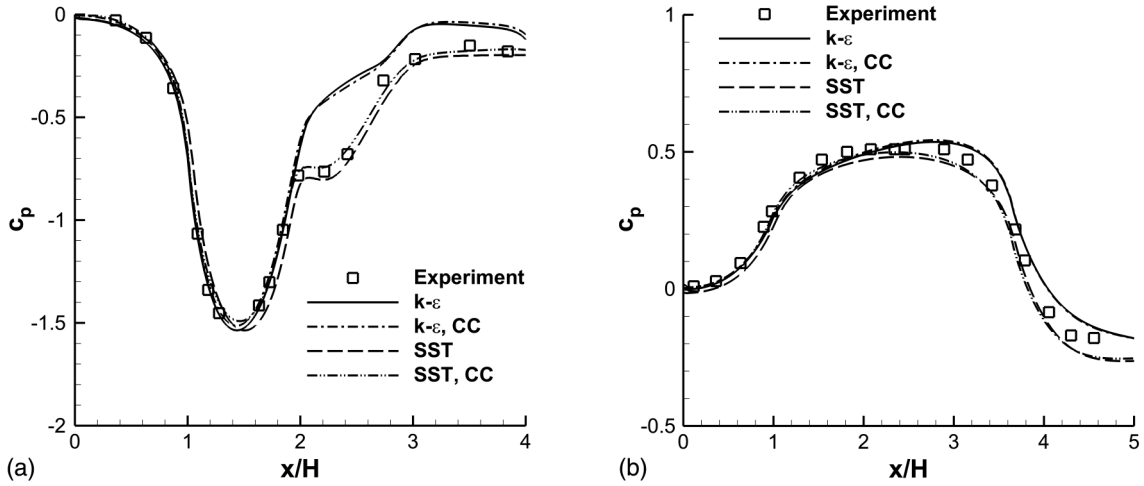

Fig. 3. Pressure coefficient on convex (a) and concave (b) surfaces of 90° duct with square cross section. Symbol *CC* stands for curvature correction term active.

(with and without the curvature-correction term) (Smirnov and Menter 2009) is performed for simulation of flow through a 90° bend duct with a square cross section. The purpose is to select the most reliable eddy-viscosity–based model for shape optimization of the air-delivery duct. The simulation results were compared with experiments by Mokhtarzadeh-Dehghan and Yuan (2002). We selected this test case due to similarities in the flow topology and the Reynolds numbers in the present study and the reference experiments (Mokhtarzadeh-Dehghan and Yuan 2002). Notice that the Reynolds number, based on mean velocity and duct height was equal to $\mathrm{Re} = 3.6 \times 10^5$ in Mokhtarzadeh-Dehghan and Yuan (2002), whereas it is $\mathrm{Re} = 3.8 \times 10^5$ (mean velocity at the duct inlet and hydraulic diameter) in our work. The reference simulations were performed on high-quality grids with $y^+ < 1$ at all walls. The inlet profiles of the mean velocity and the modeled scalars were obtained from a precursor simulation of developing flow in a straight duct with the same cross section as in Mokhtarzadeh-Dehghan and Yuan (2002). It was ensured that the proper thickness of the boundary layers was reproduced at surfaces of a straight duct and the same turbulence level was reported in the core of the flow, as in reference experiment. Fig. 3 shows a comparison between the predicted and measured pressure coefficient, $c_p = (p - p_1)/(0.5\rho U_0)$ on convex (a) and concave (b) surfaces of the duct. Here, p is the static pressure at the surface, p_1 is the reference static pressure at inlet section and U_0 is the mean velocity. The standard k-ε model underpredicts the size of the separation bubble on the convex surface. Much better results are obtained with the k-ω SST model. One can see that the role of the curvature-correction term (results denoted by CC symbol) is small in both the k-ϵ and the k-ω SST models. Nevertheless, somewhat better results were obtained with the SST model with the curvature-correction term active than using the unmodified SST model, so the former model was selected for a shape optimization of the air-delivery duct.

Mesh Deformation

In the case of our duct, the improvement of the flow characteristics (the pressure drop and flow uniformity) can be obtained only by changing the duct surface shape. The inlet part of the duct is fixed (notice a dark gray surface in Fig. 4). The geometric constraint—a bar being a part of the engine mounting (Fig. 1) limits the deformations to the duct surface.

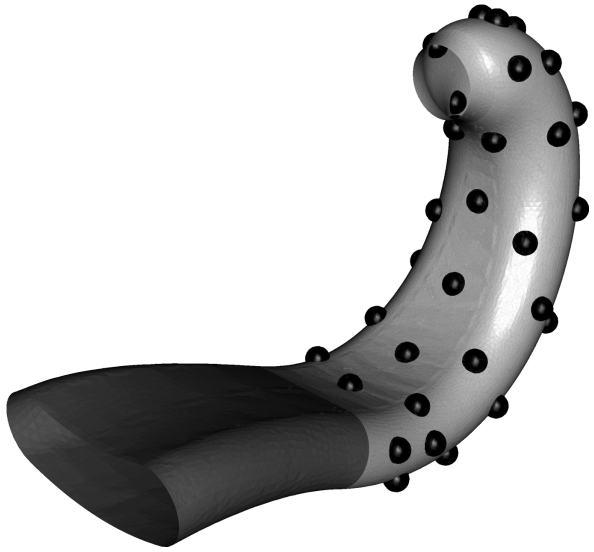

Fig. 4. Air-delivery duct with morphing points marked with black spheres. Inlet part of duct, indicated by dark gray color, is fixed and cannot be moved.

Naturally, the modification of the duct surface results in modification of the computational mesh. It is essential that the quality parameters (e.g., y^+) of the new mesh would be as good as the parameters for the base mesh. That is why we move the nodes of the existing mesh to fit the new geometry instead of remeshing the whole duct. We employ the technique of morphing points. The morphing points are placed on the surface of the duct, and their movement is transferred to the whole mesh. Fig. 4 shows the morphing points on the duct surface. The points are allowed to move only in the directions perpendicular to the surface. The movement affects all nodes, but the displacement decreases exponentially with the distance from the morphing point. The movement of one morphing point cannot affect other morphing points. It means that the displacement of each morphing point is one design variable.

In Fig. 5 we can see a cross section in the symmetry plane of the duct. The morphing points that are located on this plane are marked

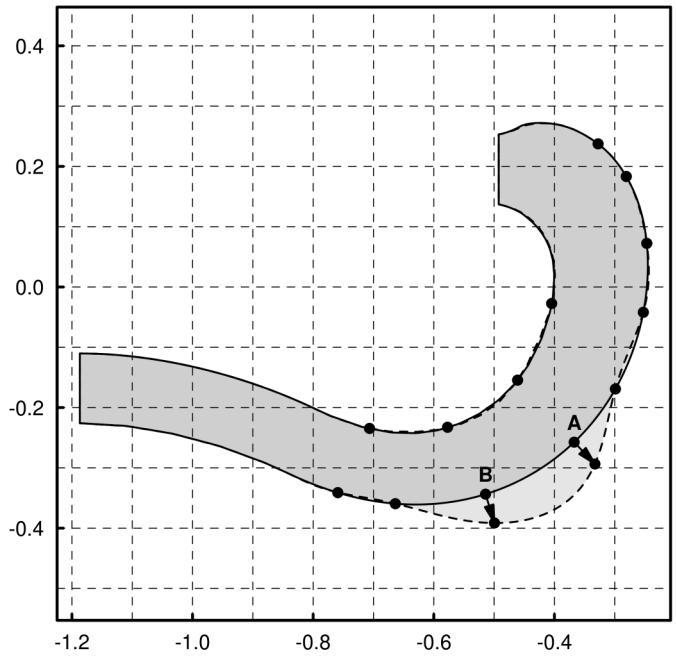

Fig. 5. Cross section in symmetry plane of duct. Result of moving both points *A* and *B* is marked with dashed line.

with black dots. The base geometry is marked with the solid line, the modified with the dashed line. The modified surface, resulting from movement of points *A* and *B* is marked with a dashed line (the deformation is magnified 10 times).

This approach is described in more detail by Łaniewski-Wołłk (2013).

Optimization

The optimization process of the considered duct is subject to certain limitations. First, the flow through the duct is simulated by the external solver. It means that we cannot introduce any modifications into the numerical code. We can provide the computational mesh and the initial conditions; the solver provides simulation results only. Second, the time needed for the solver to converge is high (roughly a day and a half on a machine equipped with 32 cores). For these two reasons, the optimization process should be largely independent of the numerical method used to simulate the flow and use as little evaluations of the objective function as possible. That is why we based a framework of the optimization on the response surface method (also called the surrogate model approach). It allows one to construct an approximation of a multidimensional function based on taken samples and use it to estimate the location of the optimum. From the variety of surrogate model methods, we chose the Kriging method (Krige 1951) [sometimes called a Gaussian process regression method (Rasmussen and Williams 2006)] because it has a strong statistical basis. It allows one to calculate not only the approximation of the unknown objective function but also the uncertainty of this approximation. The ability to consider this uncertainty is the main difference that distinguishes the Kriging method from the radial basis method.

Of course, the approximation is as good as the model. The fundamental factor influencing the model is the number of measurements used to create it. In most cases, when we have more points, we get a better model. At the same time, we cannot sample the objective function extensively because its evaluation is an expensive process. That is why we start from a small number of samples and add new ones during the optimization process. We chose the points that allow us to indicate the location of the global minimum with reasonable accuracy. The points are indicated by a sampling criterion, which is discussed in a subsequent section.

In the case of our optimization algorithm, the aim is to run several CFD computations simultaneously. We achieved this by ensuring that the criterion used for enhancing the Kriging model is capable of delivering several different sample points. The process is asynchronous—to generate a new sample point, the algorithm does not have to wait for all ongoing simulations to finish. A new sample point is generated whenever the computational resources are available, and a maximal number of parallel computations is not exceeded.

The key elements of the optimization process are described in the following sections. Here, we provide the reader with the main steps of the optimization process:

1. Initialization:
   a. Select the set of designs using the Design of Experiments technique.
   b. Calculate the objective function values for all elements of the set.
   c. Construct the Kriging model based on the results of the calculations.
2. Optimization:
   a. Choose a number of parallel evaluations of the objective function.
   b. Select the desired number of new designs using the Kriging model and a sampling criterion.
   c. Start to evaluate the objective function values for the new designs.
   d. Update the Kriging model whenever any of the evaluations are finished, and apply the sampling criterion to generate another design for evaluation.
   e. Continue with the parallel evaluations until the satisfactory design is obtained, or limit of the evaluations is reached.

Design of Experiments

Our knowledge about the function that we want to optimize is initially very limited. At the beginning of the optimization process, we only assume some properties of the objective function, e.g., its class of differentiability and variables range. Obviously, this information alone cannot be used to create the Kriging model. We need an initial set of sample points that is used to fit the model. These points lie in a sample space S, which is defined by the variables range. The process of selecting the points is called the Design of Experiments. We denote the set of sample points as $X = \{\mathbf{x}^i : i = 1, \ldots, N\}$. The number of points N necessary to fit the model should be large enough to describe the main features of the objective function properly. The minimal number of points necessary to fit the Kriging model is equal to a number of its degrees of freedom. The exact number depends on the trend function, which is used to create the model and is discussed in the following subsection. Additional points may be added during the Design of Experiments if computational resources and time is available.

The initial points should be chosen with some level of randomness and should be evenly distributed at the same time. Currently popular methods include the group of Latin hypercube sampling methods [see e.g., (Stein 1987)] and maximum projection designs [see e.g., (Joseph et al. 2015)]. We use the Latin hypercube sampling method implemented in R-package *lhs* (Carnell 2016).

Kriging Model

In the Kriging method, it is assumed that the unknown objective function f of the L-dimensional variable $\mathbf{x} = (x_1, \ldots, x_L)$ is a realization of the square-integrable random field $F(\mathbf{x})$. The random field is the sum of a deterministic trend function $\mu(\mathbf{x})$ and a centered random process $\varepsilon(\mathbf{x})$

$$F(\mathbf{x}) = \mu(\mathbf{x}) + \varepsilon(\mathbf{x}) \tag{5}$$

A form of the trend function is assumed to be a linear combination of base functions $h_p(\mathbf{x})$

$$\mu(\mathbf{x}) = \sum_{p=1}^{P} \beta_p h_p(\mathbf{x}) = \mathbf{h}^T \boldsymbol{\beta} \tag{6}$$

where $\boldsymbol{\beta} = (\beta_1, \ldots, \beta_P)$ is a vector of real coefficients in which values are estimated in a process of deriving the Kriging model. The process $\varepsilon(\mathbf{x})$ is assumed Gaussian and is completely characterized by the covariance kernel $r(\mathbf{x}, \mathbf{x}')$. Frequently this kernel is chosen as stationary, i.e., it depends only on the difference $\mathbf{x} - \mathbf{x}'$. We can write that

$$\varepsilon(\mathbf{x}) \sim \mathbb{GP}(0, r(\mathbf{x}, \mathbf{x}')) \tag{7}$$

Let us recall now the set of sample points $\mathrm{X} = \{\mathbf{x}^i : i = 1, \ldots, N\}$ (e.g., chosen in the Design of Experiments step). These points are used to:

- evaluate the objective function providing the vector of measurements

$$\mathbf{f} = (f^1, \ldots f^N) = (f(\mathbf{x}^1), \ldots, f(\mathbf{x}^1))$$

- calculate the covariance function values for each pair $\mathbf{x}^i$, $\mathbf{x}^j$, giving a covariance matrix $\mathbf{R} = (r(\mathbf{x}^i, \mathbf{x}^j))_{1 \le i \le N}^{1 \le i \le N}$; and
- calculate the base functions values for each point $\mathbf{x}^i$ giving a matrix $\mathbf{H} = (h_j(\mathbf{x}^i))_{1 \le j \le P}^{1 \le i \le N}$.

The goal is to construct the estimator $\hat{F}(\mathbf{x})$ of the model mean response and calculate the prediction $\mathrm{m}(\mathbf{x})$ taking advantage of measurements $\mathbf{f}$

$$\mathrm{m}(\mathbf{x}) = \mathbb{E}\left(\hat{F}(\mathbf{x}) | \quad \underset{i}{\forall} \; F(\mathbf{x}^i) = \mathrm{f}^i\right) \tag{8}$$

In the Kriging approach it is assumed that such estimator:

- is a linear combination of random variables $F(\mathbf{x}^i)$

$$\hat{F}(\mathbf{x}) = \sum_{i=1}^{N} \mathrm{a}^i(\mathbf{x}) F(\mathbf{x}^i) \tag{9}$$

- is unbiased

$$\mathbb{E}(\hat{F}(\mathbf{x})) = \mathbb{E}(F(\mathbf{x})) \tag{10}$$

- has a minimal mean squared error (MSE)

$$\mathrm{MSE}(\mathbf{x}) = \mathbb{E}(\hat{F}(\mathbf{x}) - F(\mathbf{x}))^2 \tag{11}$$

In the literature, such estimator is referred to as best linear unbiased estimator (BLUE). These three assumptions lead us to classic Kriging equations:

- the prediction for the model mean response

$$\mathrm{m}(\mathbf{x}) = \mathbf{h}^T \boldsymbol{\beta} + \mathbf{r}^T \mathbf{R}^{-1} (\mathbf{f} - \mathbf{H}\boldsymbol{\beta}) \tag{12}$$

where

$$\boldsymbol{\beta} = (\mathbf{H}^T \mathbf{R}^{-1} \mathbf{H})^{-1} \mathbf{H}^T \mathbf{R}^{-1} \mathbf{f} \tag{13}$$

and

- the model variance

$$\sigma^2(\mathbf{x}) = \mathrm{r}(\mathbf{x}, \mathbf{x}) - \mathbf{r}^T \mathbf{R}^{-1} \mathbf{r} + (\mathbf{h} - \mathbf{H}^T \mathbf{R}^{-1} \mathbf{r})^T (\mathbf{H}^T \mathbf{R}^{-1} \mathbf{H})^{-1} (\mathbf{h} - \mathbf{H}^T \mathbf{R}^{-1} \mathbf{r}) \tag{14}$$

Denotations that are additionally introduced:

- a vector of basis functions values in point $\mathbf{x}$

$$\mathbf{h} = (h_1(\mathbf{x}), \ldots, h_P(\mathbf{x}))$$

- a vector of covariance function values for each pair $\mathbf{x}$, $\mathbf{x}^i$

$$\mathbf{r} = (r(\mathbf{x}, \mathbf{x}^1), \ldots, r(\mathbf{x}, \mathbf{x}^N))$$

To make the Kriging model complete we have to choose a type of covariance kernel $r(\mathbf{x}, \mathbf{x}')$ and trend functions $h_p(\mathbf{x})$. This choice represents our initial knowledge about the objective functions that we want to optimize. If we assume an inappropriate type of the kernel or the trend function, the optimization process can be excessively time-consuming and may lead to suboptimal results.

In the present study, we use the Gaussian kernel. It is our experience that one can expect a high level of smoothness in flow cases similar to this one. In one dimension this kernel has a following form:

$$c_{1d}(x_l, x_l'; \theta_l) = \exp\left(-\frac{(x_l - x_l')^2}{2\theta_l^2}\right) \tag{15}$$

The parameter θ_l is called a covariance radius and controls how strong the correlation is in lth dimension between the points $\mathbf{x}$ and $\mathbf{x}'$. In many dimensions it is usual to take a tensor product of such kernels

$$r(\mathbf{x}, \mathbf{x}'; \boldsymbol{\theta}, \sigma^2, \tau^2) = \sigma^2 \prod_{l=1}^{L} c_{1d}(x_l, x_l'; \theta_l) + \tau^2 \delta_{\mathbf{x},\mathbf{x}'} \tag{16}$$

where

$$\delta_{\mathbf{x},\mathbf{x}'} = \begin{cases} 1, & \mathbf{x} = \mathbf{x}' \\ 0, & \mathbf{x} \neq \mathbf{x}' \end{cases} \tag{17}$$

The parameter σ^2 is a multiplier that scales the model variance and is referred to as a process variance. The parameter τ^2 is called a nugget and is added to the covariance kernel to handle situations when the output of the simulator may be noisy. In our case, as the solver is deterministic, we obtain the same objective function values for the simulations repeated in the same conditions, but a small change in conditions, particularly in the geometry, may result in a significant change in simulation outputs resulting in the discontinuity of the objective functions. The addition of the nugget effect handles these discontinuities. The Kriging prediction is still interpolating the measurements, but the prediction is smoother outside the set X and the model variance is larger. One can also choose to add an uncorrelated random error on top of the Kriging model achieving regression but not interpolation.

To find values of all mentioned parameters $\boldsymbol{\theta}$, σ^2, and τ^2 a maximum likelihood estimate method is frequently used. In this approach, a likelihood function is constructed. It expresses our certainty that a statistical model predicts values that are observed. In the case of the Gaussian process the likelihood function is of the form

$$\mathrm{L} = \frac{1}{(2\pi)^{N/2}|\mathbf{R}|^{1/2}} \exp\left(-\frac{1}{2}(\mathbf{f} - \mathbf{H}\boldsymbol{\beta})^T \mathbf{R}^{-1}(\mathbf{f} - \mathbf{H}\boldsymbol{\beta})\right) \tag{18}$$

The goal is to find the parameters' values for which the maximum of this function occurs. To do that we use an optimization algorithm implemented in *DiceKriging* R-package (Roustant et al. 2012).

There is a variety of functions from which the trend function can be chosen. We decided to use a linear function of dimensions

$$\mu(\mathbf{x}) = \beta_0 + \sum_{j=1}^{L} \beta_j x_j \tag{19}$$

This function has only $L + 1$ degrees of freedom. It is also the minimal number of points that should be generated during the Design of Experiments and allows moderate evaluation of the objective function.

Sampling Criterion

Because of our limited knowledge about the objective function, the sample points are selected using the Latin hypercube sampling method at the beginning of the optimization. As soon as the first surrogate model is constructed, we can use it to formulate a criterion, which can indicate the subsequent points. When the first model is built this limitation no longer exists; we can use it to formulate a criterion that can indicate the subsequent points. The sampling criterion should allow us to find the global optimum of the objective function with good accuracy and a reasonable amount of computational resources.

A method that is frequently employed to indicate the sample points is called the Expected Improvement method. It allows us to balance a search for a global and local minimum, leading to an Efficient Global Optimization algorithm proposed by Jones et al. (1998). The approach itself dates from the 1970s [see e.g., (Mockus et al. 1978)]. The algorithm is based on the following function:

$$\mathrm{EI}(\mathbf{x}) = \mathbb{E}\left(\max_{\mathbf{x}\in S}(f_{\min} - \hat{F}(\mathbf{x}), 0)\right) \tag{20}$$

where $f_{\min}$ is the minimum of the already evaluated objective function values. The expression $\max(f_{\min} - \hat{F}(\mathbf{x}), 0)$ is the actual improvement in the point $\mathbf{x}$. The expected improvement function is equal to zero at points in which the objective function is already evaluated and is nonnegative elsewhere. A point for which the maximum of the expected improvement function occurs is a candidate for the new sample point. However, the mentioned method can be used only in the case of single-objective optimization problems. A multiobjective sampling criterion is used to address this problem.

Different approaches were developed to address a problem of the multiobjective optimization. Their aim is to measure the quality of possible designs $\mathbf{x}$ allowing the selection of the best one. Each design is characterized by a set of objective function values (also referred to as the outcome). Thus, the most straightforward solution is to map the values of the objective functions for each sample point to a single value. This makes it possible to compare the designs in a direct way. To do that a so-called indicator function should be defined. A description of common approaches to the multiobjective optimization based on indicator functions is provided in the thesis by Parr (2013). Frequently, a hypervolume is chosen as such an indicator. The volume is delimited by the values of the objective functions for the possible design and the values of the objective functions for a reference design. The calculation of the hypervolume in many dimensions is time-consuming and various numerical methods are used to do it efficiently. A comparison of such methods is provided, e.g., in the thesis by Bradstreet (2011).

A standard approach in multiobjective optimization is to select a set of optimal designs instead of one design. These designs correspond to outcomes for which we cannot improve the value of any objective function without worsening at least one another objective. Such outcomes are called Pareto optimal or nondominated. When the new outcome is also nondominated, it means that at least one objective function value is improved. For such new nondominated points, one can calculate how much it improves the hypervolume compared to the current Pareto front. Still, the optimization based on the Pareto front and the hypervolume is insufficient. The Kriging response is the random variable, and as a consequence, the hypervolume is the random variable too. We have to take its expected value to obtain a single number. It leads us to the Expected Hypervolume Improvement method. This approach was considered, e.g., by Emmerich (2005) and Łaniewski-Wołłk (2010).

To formulate a quantitative criterion, we have to introduce new definitions. Our optimization problem is described by the objective functions $f_1(\mathbf{x})$–pressure loss and $f_2(\mathbf{x})$–flow uniformity. These functions are evaluated at the sample points $\mathbf{x}^i$. Each pair of obtained values, denoted as $p^i = (f_1(\mathbf{x}^i), f_2(\mathbf{x}^i))$, is a point in the outcome space. These points create a set P corresponding to the set of sample points X.

As the reference point we chose the objective function values for the base design $t = (f_1(\mathbf{x}^0), f_2(\mathbf{x}^0))$. The reference level t can be very useful because it can be used to narrow the region of the Pareto front that the optimization algorithm explores.

We define the hypervolume function $\mathrm{HV}_t(P)$ as the two-dimensional (2D) volume of the set of points dominated by P and dominating t. A point for the possible design, defined by the mean response estimators of the objective functions, is denoted as $\hat{p}(\mathbf{x}) = (\hat{F}_1(\mathbf{x}), \hat{F}_2(\mathbf{x}))$. Now we can write the function for the Expected Hypervolume Improvement

$$\mathrm{EHVI}(\mathbf{x}) = \mathbb{E}(\mathrm{HV}_t(P \cup \{\hat{p}(\mathbf{x})\}) - \mathrm{HV}_t(P)) \tag{21}$$

where

- $\mathrm{HV}_t(P)$ is a volume created by the current Pareto set; and
- $\mathrm{HV}_t(P \cup \{\hat{p}(\mathbf{x})\})$ is the volume after adding the point $\hat{p}(\mathbf{x})$.

The evaluation of this function can be computationally expensive. However, if the components of $\hat{p}(\mathbf{x})$ are independent random variables, the computation can be reduced to a single deterministic hypervolume computation, for which there are proven algorithms.

First, let us introduce additional definitions. For a point $p \in \mathbb{R}^2$, we define $\mathrm{D}^-(p) = \{v \in \mathbb{R}^2: \quad \forall_i\ v_i < p_i\}$ as the lower dominated set and $\mathrm{D}^+(p) = \{v \in \mathbb{R}^2: \quad \forall_i\ v_i > p_i\}$ as the upper dominated set. For a set $P \subset \mathbb{R}^2$ we define $\mathrm{D}^+(P) = \cup_{p\in P}\ \mathrm{D}^+(p)$. The standard Lebesgue measure is denoted as $|\cdot|$. We can write the formula for the Expected Hypervolume Improvement [defined in Eq. (21)]

$$\mathrm{EHVI}(\mathbf{x}) = \mathbb{E}|\mathrm{D}^-(t) \cap (\mathrm{D}^+(P) \cup \mathrm{D}^+(\hat{p}))| - \mathbb{E}|\mathrm{D}^-(t) \cap \mathrm{D}^+(P)| \tag{22}$$

After a transformation we obtain

$$\mathrm{EHVI}(\mathbf{x}) = \mathbb{E}|\mathrm{D}^-(t) \cap \mathrm{D}^+(\hat{p})| - \mathbb{E}|(\mathrm{D}^-(t) \cap \mathrm{D}^+(P)) \cap \mathrm{D}^+(\hat{p}))| \tag{23}$$

One can view this calculation, as a difference of volumes of two sets with respect to a new measure defined as $\mu(\Omega) = \mathbb{E}|\Omega \cap \mathrm{D}^+(\hat{p})|$. This measure can be expressed as

$$\begin{aligned}\mu(\Omega) &= \mathbb{E}|\Omega \cap \mathrm{D}^+(\hat{p})| \\ &= \mathbb{E}\iint \mathbf{1}_{\mathrm{D}^+(\hat{p})}(x)\mathbf{1}_{\Omega}(x)dx_1dx_2 \\ &= \iint \mathbb{E}(\mathbf{1}_{\mathrm{D}^+(\hat{p})}(x))\mathbf{1}_{\Omega}(x)dx_1dx_2 \end{aligned} \tag{24}$$

where $\mathbf{1}_A(x)$ is the indicator function, equal to 1 for $x \in A$ and 0 otherwise. Moreover, $\mathbb{E}(\mathbf{1}_A(X)) = \mathbb{P}(X \in A)$, in which $\mathbb{P}$ is the probability. In the case of the independent variables, we get

$$\begin{aligned}\mu(\Omega) &= \iint \mathbb{P}(x \in \mathrm{D}^+(\hat{p}))\mathbf{1}_{\Omega}(x)dx_1dx_2 \\ &= \iint \mathbb{P}(x_1 \geq \hat{p}_1)\mathbb{P}(x_2 \geq \hat{p}_2)\mathbf{1}_{\Omega}(x)dx_1dx_2 \end{aligned} \tag{25}$$

Now, let us define a transformation Γ_X as an integral of a cumulative distribution function: $\Gamma_X(z) = \int_{-\infty}^{z}\mathbb{P}(x \geq X)dx$. The application of $\Gamma_{\hat{p}_1}$ and $\Gamma_{\hat{p}_2}$ to the respective components of x is denoted as $\Gamma_{\hat{p}}(x)$. Furthermore, the transformation is injective ($\Gamma_{\hat{p}}(x) \in \Gamma_{\hat{p}}(\Omega) \Leftrightarrow x \in \Omega$) wherever $\mathbb{P}(x_1 \geq \hat{p}_1)$ and $\mathbb{P}(x_2 \geq \hat{p}_2)$ are nonzero.

We can use this transformation as a substitution in the integral

$$\begin{aligned}\mu(\Omega) &= \iint \Gamma'_{\hat{p}_1}(x_1)\Gamma'_{\hat{p}_2}(x_2)\mathbf{1}_{\Gamma_{\hat{p}}(\Omega)}(\Gamma_{\hat{p}}(x))dx_1dx_2 \\ &= \int_0^{\infty}\int_0^{\infty}\mathbf{1}_{\Gamma_{\hat{p}}(\Omega)}(y)dy_1dy_2 = |\Gamma_{\hat{p}}(\Omega)| \end{aligned} \tag{26}$$

where $\Gamma_{\hat{p}}(x)$ means an application of $\Gamma_{\hat{p}_1}$ and $\Gamma_{\hat{p}_2}$ to the respective components of x. Moreover, the transformation Γ is always increasing and transforms $-\infty$ to 0. This gives us

$$\begin{aligned}\mathrm{EHVI}(\mathbf{x}) &= \mu(\mathrm{D}^-(t)) - \mu(\mathrm{D}^-(t) \cap \mathrm{D}^+(P)) = \\ &= |\Gamma_{\hat{p}}(\mathrm{D}^-(t))| - |\Gamma_{\hat{p}}(\mathrm{D}^-(t) \cap \mathrm{D}^+(P))| = \\ &= |\mathrm{D}^-(\Gamma_{\hat{p}}(t)) \cap \mathrm{D}^+((0,0))| \\ &\quad - |\mathrm{D}^-(\Gamma_{\hat{p}}(t)) \cap \mathrm{D}^+(\Gamma_{\hat{p}}(P))| = \\ &= \mathrm{HV}_{\Gamma_{\hat{p}}(t)}(\{(0,0)\}) - \mathrm{HV}_{\Gamma_{\hat{p}}(t)}(\Gamma_{\hat{p}}(P)) \end{aligned} \tag{27}$$

This result reduces the Expected Hypervolume Improvement computation to: transforming both the reference level t and the Pareto front P with the Γ transform (each coordinate separately), and subtracting hypervolume of the Pareto front from the volume of 0 to t hypercube. For the hypervolume computation we use the function dominated Hypervolume from the R package mco (Mersmann et al. 2014). The package implements the algorithm described by Fonseca et al. (2006), which has a complexity of $O(n)$ for 2D and $O(n^{d-2}\log n)$ for $d > 2$ dimensions.

The described algorithm was developed originally for a 2010 study by one of the authors (Łaniewski-Wołłk 2010) and used in an open source optimization package (Łaniewski-Wołłk 2016), which was made public by the authors. Such complexity for the Expected Hypervolume Improvement computation improves upon the complexity reported by Hupkens et al. (2015), and is even with the 3D algorithm reported by Yang et al. (2017).

It is interesting to note that the $\Gamma_X(z)$ transformation coincides with a version of Expected Improvement: $\Gamma_X(z) = \mathbb{E}(\max(z - X, 0))$.

To find a candidate for the new sample point we have to find the maximum point of this function. It implies the optimization of the highly multimodal function, which is characterized by many local optima. In such cases, the evolutionary algorithm is frequently used. This is frequently inefficient, as the Expected Hypervolume Improvement (similar to Expected Improvement) has wide regions in which its value is nearly zero. To tackle this problem, we decided to perform the multiobjective optimization involving the simultaneous optimization of the Expected Hypervolume Improvement function and predictions $m_1(\mathbf{x})$ and $m_2(\mathbf{x})$ for the two Kriging models. To optimize this subproblem, we use the multiobjective algorithm NSGA II implemented in the mco package (Mersmann et al. 2014). The evaluations of these functions are fast in comparison with the evaluation of the real objective functions. Hence, we can use a relatively large population and large number of iterations to obtain an accurate Pareto front. Finally, as the new design, we chose a point with the maximum Expected Hypervolume Improvement value.

Robust Parallel Optimization

In the case of computational fluid dynamics analyses, calculation of the single value of the objective function can be very time-consuming. Optimization process based on sequential evaluations may be excessively long. The solution to this problem is to perform parallel evaluations of the objective function. Such calculations are run in batches (synchronous optimization) or conducted asynchronously. The work by Ginsbourger et al. (2010) describes the synchronous optimization based on Gaussian processes and Janusevskis et al. (2012) formulate optimization criteria for the asynchronous process. To make our optimization algorithm parallel the sampling criterion should be modified. Instead of indicating one candidate for a sample point, the criterion should indicate a few of them. It is important to mention that these points should not form clusters. We want to keep a balance between the search for the global and local optimum. First, we make an observation that the Expected Hypervolume Improvement is equal to zero in points that are already evaluated. In consequence, the sampling algorithm will not indicate the new points in neighborhoods of the old ones. We utilize this property by assuming that the result of the ongoing calculation of the objective function will be the same as the prediction of the Kriging model. Then we create the new Kriging model and use the sampling criterion to indicate another sample point. This procedure can be repeated until we obtain the required number of parallel evaluations of the objective function. More importantly, we do not have to wait for ongoing calculations to finish. We can add the new sample point whenever any of the previous function evaluations finishes. It makes our algorithm asynchronous.

In the literature, the described approach is sometimes called the Kriging believer heuristic (Ginsbourger et al. 2010). The Kriging model predictions, which replace the results of the ongoing calculations, are sometimes called the hallucinations (Desautels et al. 2014).

The described approach makes our algorithm resistant to solver or mesh failures. When such a situation happens for a certain sample point, we assume that the corresponding objective function value is equal to the prediction of the Kriging model in this point. It prevents the sampling algorithm from indicating new points in its neighborhood. At the same time, this approach does not stop the whole optimization process.

Detection of the subregions of the design space in which the solver or mesh failures occurs is sometimes treated as a separate classification problem. Such approach is described, e.g., by Sacher et al. (2018) and Tran et al. (2019).

Results

Optimization Conditions

The described methodology was applied to the case of the air-delivery duct. Our goal was to modify its shape to achieve the minimal pressure loss Δp_l across the duct and the improved/not-worsen flow uniformity expressed by the distortion coefficient DC_{60}. It was important for us that the flow uniformity was not deteriorated. In such conditions, a constrained single-objective optimization, in which the pressure loss is the objective function, and the flow uniformity is the constraint, could be employed. Nevertheless, from our experience, the Pareto front provides an engineer with much more data and allows making better decisions. In our case, if we would have the uniformity as the constraint, we could omit designs that have a similar pressure loss but better uniformity.

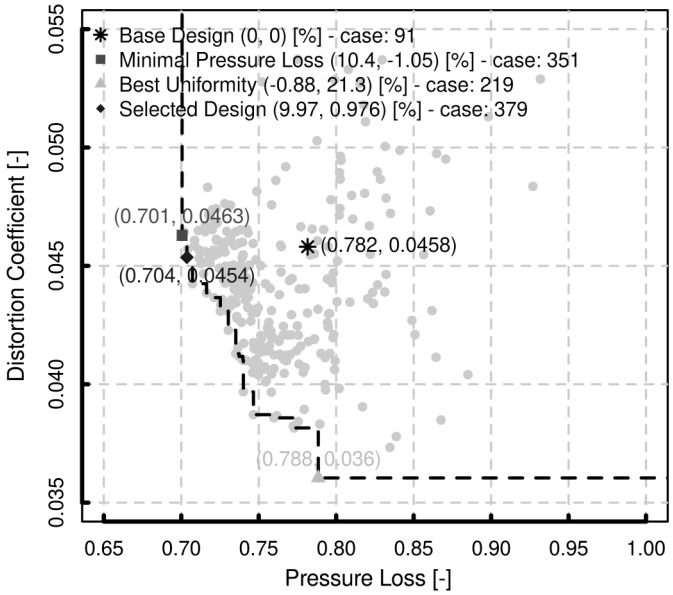

Fig. 6. Pareto front obtained in optimization process. Legend contains information about improvement of each design with respect to base design.

We introduced the $L = 30$ design variables (Fig. 4), which controlled the mesh deformation. Each of the variables could vary within the range $[-0.32,0.32]$[cm].

To fit the initial Kriging model, we needed enough points to remove all of its degrees of freedom. In the case of the linear trend function this number is equal to $L + 1 = 31$. We selected a larger number of the sample points (90) due to available computational resources. To do this we used a Latin hypercube sampling method (Stein 1987) implemented in the R package *lhs* (Carnell 2016). We chose the genetic LHS function, which takes advantage of the S-criterion optimization algorithm (Stocki 2005).

For each sample point, the simulation was performed. If any evaluation failed, a corresponding point was marked accordingly.

The initial points and the results of the evaluation were used in further optimization. We prepared the Kriging models based on all evaluations. In the case of the simulations that failed or did not yet finish, we used the Kriging predictors to *substitute* for the missing objective function values (Kriging believer heuristic). The Expected Hypervolume Improvement criterion was used to find a new sample point. This step was repeated whenever any of the previous simulations finished, and the number of five parallel evaluations was not exceeded. It means that the entire optimization process was

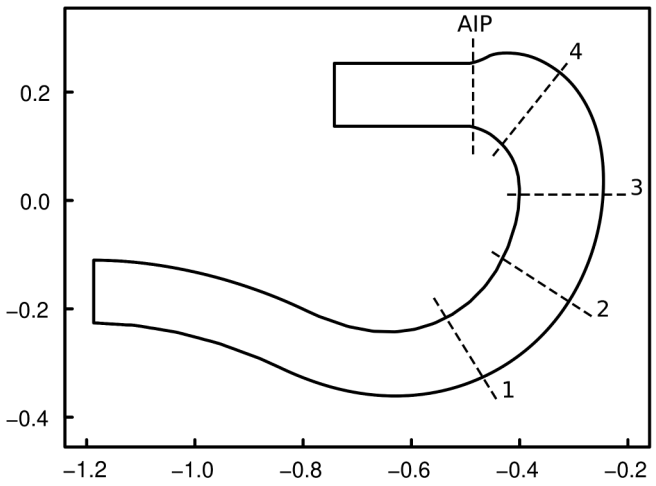

Fig. 8. View of duct in symmetry plane. Cross sections across flow through duct are marked with dashed lines.

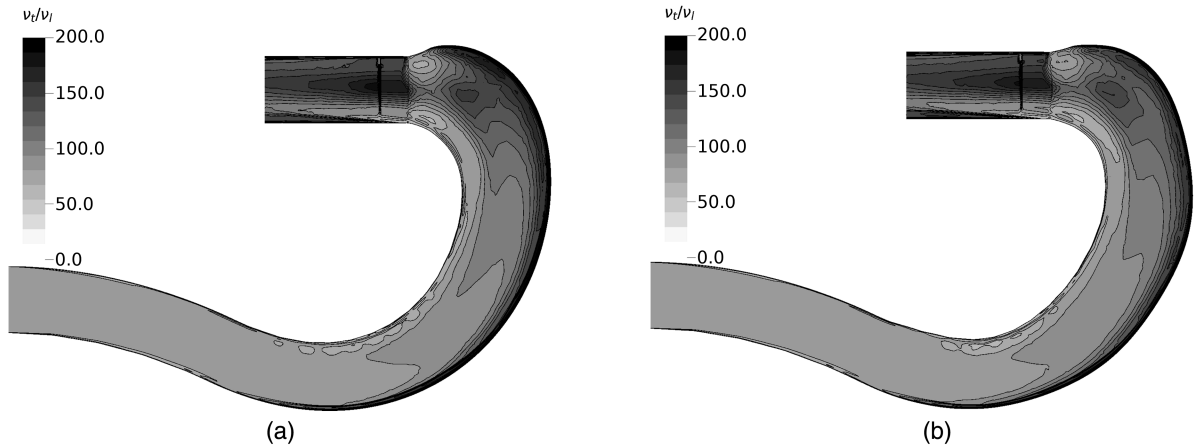

Fig. 7. Contour plots of turbulent to molecular viscosity ratio ν_t/ν in symmetry plane for base (a) and selected (b) design.

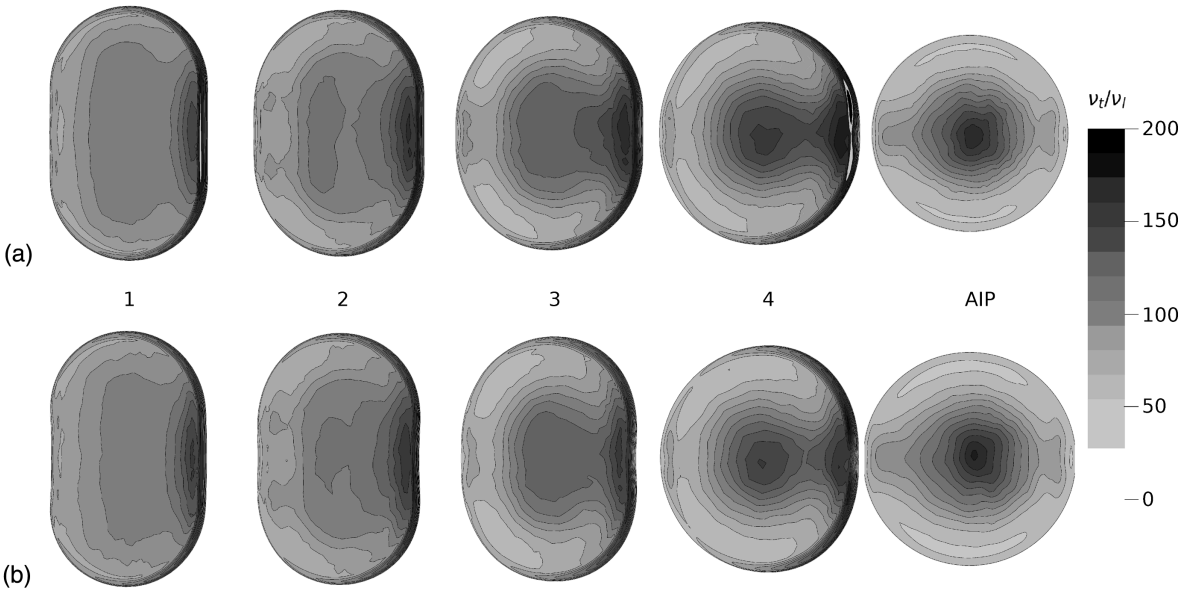

Fig. 9. Contour plots of turbulent to molecular viscosity ratio in selected cross sections of base (a); and selected (b) design.

parallel and asynchronous. With this approach, we performed a total of 380 evaluations of the objective functions. During the Design of Experiments step, 36 evaluations out of 90 were unconverged. The optimization based on the EHVI criterion resulted in 60 unconverged evaluations out of 229.

Optimal Designs

We show the Pareto front obtained in the optimization process in Fig. 6. On the horizontal axis we plot the dimensionless pressure loss

$$\Delta\tilde{p}_l = \frac{\Delta p_l}{0.5 \cdot \rho_{\text{avg}} \cdot v_{\text{avg}}^2} \tag{28}$$

where ρ_{avg} and v_{avg} are respectively an area-averaged density and an area-averaged velocity at the duct inlet. On the vertical axis, the DC_{60} distortion coefficient is shown.

The base design is marked with a star, a design for which we achieved the minimal pressure loss is marked with a square, a triangle indicates the best uniformity design and a rhomboid indicates a selected design.

We focus on the design denoted as selected design in Fig. 6. The reduction in the value of the pressure loss is our primary objective. As for the uniformity, we seek only for a design for which the value of the uniformity is not worse than the base design. Design number 379 fulfills these two requirements and is selected for further analysis.

In the case of the selected design, the pressure loss is lower than 10% with respect to the pressure loss for the base design.

In Fig. 7 we can see the turbulent to molecular viscosity ratio ν_t/ν in the symmetry plane for the base (a) and selected (b) designs. We can see that, for the selected design, the ratio is smaller near the concave duct surface.

It is well known that a convex surface is characterized by better flow stabilization characteristics and lower turbulence production (Smirnov and Menter 2009) than the concave surface. As shown in Fig. 7(b) the optimization algorithm tries to change the shape of the outer part of the air-delivery duct in such a way that it becomes less concave with respect to the baseline design [Fig. 7(a)].

In order to further inspect the evolution of the turbulent to molecular viscosity ratio inside the duct, the cuts are made in planes perpendicular to the main flow, as shown in Fig. 8. The contour plots of ν_t/ν are shown in Fig. 9 for the baseline (a) and modified (b) cases. One can notice some changes in the modified surface shape on the bottom part of the duct in cross section number 3, and in the upper part of the surface in the cross section number 4. Again, the optimization algorithm tries to modify the surface shape, so it becomes less concave with respect to the baseline design. This leads to reduced turbulence activity in the vicinity of the duct surface and results in the reduced total pressure loss in the improved design.

Conclusion

In the paper, we describe the aerodynamic optimization of the duct surface shape. The duct is a part of the turboprop engine air-delivery system. Two objectives are defined, namely the minimization of the pressure loss across the duct and the maximization of the flow uniformity at the duct outlet. We have reached the goals by changing the shape of the duct while taking into account the geometrical constraints. The optimization is based on the Kriging models. We parallelized the process and made it asynchronous. This way, the optimization algorithm does not need to wait for all ongoing calculations to finish, but generates a new candidate for simulation when needed. The process is resistant to solver and mesh failures. This property is particularly important when the optimization of complex flow problems is necessary. The proposed method allowed to decrease the pressure loss on the optimized geometry by 10% with respect to the baseline design.

Data Availability Statement

Some or all data, models, or code generated or used during the study are available in a repository or online in accordance with funder data retention policies (Łaniewski-Wołłk 2016, "ASynchronious Efficient Multiobjective Optimization," GitHub repository, https://github.com/llaniewski/ASEMOO).

Some or all data, models, or code used during the study were provided by a third party (the base design of the air-delivery duct). Direct requests for these materials may be made to the provider as indicated in the Acknowledgments.

Acknowledgments

The authors would like to thank W. Stalewski and J. Żółtak, who provided the base design of the air-delivery duct (Stalewski and Żółtak 2014). This work was partly prepared under the ESPOSA (Grant No. FP7-AAT-2011-RTD01 284859) and UMRIDA (Grant No. ACP3-GA-2013-605036) projects.

References

Alessi, G., L. Koloszar, T. Verstraete, and J. P. A. J. van Beeck. 2019. "Node-based adjoint surface optimization of u-bend duct for pressure loss reduction." *Comput. Methods Appl. Sci.* 49: 61–75. https://doi.org/10.1007/978-3-319-89890-2_5.

Aranake, A., J. G. Lee, D. Knight, R. Cummings, J. Cox, M. Paul, and A. Byerley. 2011. "Automated design optimization of a three-dimensional subsonic diffuser." *J. Propul. Power* 27: 838–846. https://doi.org/10.2514/1.50522.

Bae, H., S. Park, and J. Kwon. 2012. "Efficient global optimization for S-duct diffuser shape design." *J. Aerosp. Eng.* 227 (9): 1516–1532. https://doi.org/10.1177/0954410012457891.

Bradstreet, L. 2011. "The hypervolume indicator for multi-objective optimisation: Calculation and use." Ph.D. thesis, Univ. of Western Australia. https://research-repository.uwa.edu.au/en/publications/the-hypervolume-indicator-for-multi-objective-optimisation-calcul.

Carnell, R. 2016. "LHS: Latin hypercube samples." R package version 0.14. Accessed April 30, 2020. https://CRAN.R-project.org/package=lhs.

Chiereghin, N., L. Guglielmi, M. Savill, E. Manca, A. Rigobello, M. Barison, and E. Benin. 2017. "Shape optimization of a curved duct with free form deformations." In *Proc., 23rd AIAA Computational Fluid Dynamics Conf.* Denver: American Institute of Aeronautics and Astronautics.

D'Ambros, A., T. Kipouros, P. Zachos, M. Savill, and E. Benini. 2018. "Computational design optimization for S-ducts." *Designs* 2 (4): 36. https://doi.org/10.3390/designs2040036.

Desautels, T., A. Krause, and J. W. Burdick. 2014. "Parallelizing exploration-exploitation tradeoffs in gaussian process bandit optimization." *J. Mach. Learn. Res.* 15: 4053–4103.

Emmerich, M. 2005. "Single- and multi-objective evolutionary design optimization assisted by gaussian random field metamodels." Ph.D. thesis, TU Dortmund. http://hdl.handle.net/2003/21807.

Fonseca, C., L. Paquete, and M. Lopez-Ibanez. 2006. "An improved dimension-sweep algorithm for the hypervolume indicator." In *Proc., 2006 IEEE Int. Conf. on Evolutionary Computation*. Vancouver, Canada: IEEE.

Furlan, F., N. Chiereghin, T. Kipouros, E. Benini, and M. Savill. 2014. "Computational design of S-duct intakes for distributed propulsion." *Aircr. Eng. Aerosp. Technol. Int. J.* 86 (6): 473–477. https://doi.org/10.1108/AEAT-04-2014-0046.

Gan, W., and X. Zhang. 2017. "Design optimization of a three-dimensional diffusing S-duct using amodified SST turbulent model." *Aerosp. Sci. Technol.* 63 (Apr): 63–72. https://doi.org/10.1016/j.ast.2016.12.016.

Ginsbourger, D., R. L. Riche, and L. Carraro. 2010. "Kriging is well-suited to parallelize optimization." In Vol. 2 of *Computational intelligence in expensive optimization problems: Adaptation learning and optimization*, edited by Y. Tenne and C. Goh. Berlin: Springer.

Girdziusas, R., R. L. Riche, F. Viale, and D. Ginsbourger. 2012. "Parallel budgeted optimization applied to the design of an air duct." Accessed March 5, 2020. https://hal.archives-ouvertes.fr/hal-00723427.

Hupkens, I., A. Deutz, K. Yang, and M. Emmerich. 2015. "Faster exact algorithms for computing expected hypervolume improvement." In *Proc., Int. Conf. on Evolutionary Multi-Criterion Optimization*, 65–79. New York: Springer.

Janusevskis, J., R. L. Riche, D. Ginsbourger, and R. Girdziusas. 2012. "Expected improvements for the asynchronous parallel global optimization of expensive functions: Potentials and challenges." In *Learning and intelligent optimization*, edited by Y. Hamadi and M. Schoenauer. Berlin: Springer.

Jones, D. R., M. Schonlau, and W. J. Welch. 1998. "Efficient global optimization of expensive black-box functions." *J. Global Optim.* 13: 455–492. https://doi.org/10.1023/A:1008306431147.

Joseph, V. R., E. Gul, and S. Ba. 2015. "Maximum projection designs for computer experiments." *Biometrika* 102 (2): 371–380. https://doi.org/10.1093/biomet/asv002.

Krige, D. G. 1951. "A statistical approach to some basic mine valuation problems on the witwatersrand." *J. Chem. Metall. Min. Soc. S. Afr.* 52: 119–139.

Łaniewski-Wołłk, Ł. 2010. "Expected hypervolume improvement—Criterion for kriging based multiobjective optimization." In *Proc., 19th Polish National Fluid Dynamics Conf.* Poznań, Poland: Polish Academy of Sciences, Committee of Mechanics.

Łaniewski-Wołłk, Ł. 2013. "Automatic parametrization and mesh deformation for CFD optimization (November)." Accessed November 25, 2013. http://arxiv.org/abs/1311.6190v1.

Łaniewski-Wołłk, Ł. 2016. "Asynchronious efficient multiobjective optimization." Accessed October 2, 2017. https://github.com/llaniewski/ASEMOO.

Mersmann, O., H. Trautmann, D. Steuer, B. Bischl, and K. Deb. 2014. "MCO: Multiple criteria optimization algorithms and related functions." Accessed April 30, 2020. https://CRAN.R-project.org/package=mco.

Mockus, J., V. Tiesis, and A. Zilinskas. 1978. "L. c. w. dixon and g. p. szego." In *Towards global optimisation*, 117–129. Amsterdam, Netherlands: North Holland.

Mokhtarzadeh-Dehghan, M., and Y. Yuan. 2002. "Measurements of turbulence quantities and bursting period in developing turbulent boundary layers on the concave and convex walls of a 90° square bend." *Exp. Therm Fluid Sci.* 27: 59–75. https://doi.org/10.1016/S0894-1777(02)00213-3.

Namgoong, H., C. Son, and P. Ireland. 2008. "U-bend shaped turbine blade cooling passage optimization." In *Proc., 12th AIAA/ISSMO Multidisciplinary Analysis and Optimization Conf.* Victoria, Canada: American Institute of Aeronautics and Astronautics.

Parr, J. M. 2013. "Improvement criteria for constraint handling and multiobjective optimization." Ph.D. thesis, Univ. of Southampton. https://eprints.soton.ac.uk/349978/1/JPARR-Thesis.pdf.

Raghavan, B., and P. Breitkopf. 2013. "Asynchronous evolutionary shape optimization based on high-quality surrogates: Application to an air-conditioning duct." *Eng. Comput.* 29: 467–476. https://doi.org/10.1007/s00366-012-0263-0.

Rasmussen, C. E., and C. K. I. Williams. 2006. *Gaussian processes for machine learning*. Cambridge, MA: MIT Press.

Roustant, O., D. Ginsbourger, and Y. Deville. 2012. "Dicekriging, diceoptim: Two R packages for the analysis of computer experiments by kriging-based metamodeling and optimization." *J. Stat. Software* 51 (1): 54. https://doi.org/10.18637/jss.v051.i01.

Sacher, M., R. Duvigneau, O. L. Maître, M. Durand, Élisa Berrini, F. Hauville, and J.-A. Astolfi. 2018. "A classification approach to efficient global optimization in presence of non-computable domains." *Struct. Multidiscip. Optim.* 58 (4): 1537–1557. https://doi.org/10.1007/s00158-018-1981-8.

Schonlau, M. 1997. "Computer experiments and global optimization." Ph.D. thesis, Univ. of Waterloo. https://www.collectionscanada.gc.ca/obj/s4/f2/dsk3/ftp04/nq22234.pdf.

Shahriari, B., K. Swersky, Z. Wang, R. Adams, and N. de Freitas. 2015. "Taking the human out of the loop: A review of bayesian optimization." *Proc. IEEE* 104 (1): 148–175. https://doi.org/10.1109/JPROC.2015.2494218.

Smirnov, P., and F. Menter. 2009. "Sensitization of the SST turbulence model to rotation and curvature by applying the Spalart-Shur correction term." *J. Turbomach.* 131 (4): 1–8. https://doi.org/10.1115/1.3070573.

Soemarwoto, B. I., O. J. Boelens, and T. Kanakis. 2016. "Aerodynamic design of gas turbine engine intake duct." *Aircr. Eng. Aerosp. Technol.* 88 (5): 605–612. https://doi.org/10.1108/AEAT-02-2015-0063.

Stalewski, W., and J. Żółtak. 2014. "The preliminary design of the air-intake system and the nacelle in the small aircraft-engine integration process." *Aircr. Eng. Aerosp. Technol. Int. J.* 86 (3): 250–258. https://doi.org/10.1108/AEAT-01-2013-0015.

Stein, M. 1987. "Large sample properties of simulations using Latin hypercube sampling." *Technometrics* 29: 143–151. https://doi.org/10.1080/00401706.1987.10488205.

Stocki, R. 2005. "A method to improve design reliability using optimal Latin hypercube sampling." *Comput. Assisted Mech. Eng. Sci.* 12: 87–105.

Storn, R., and K. Price. 1997. "Differential evolution—A simple and efficient heuristic for global optimization over continuous spaces." *J. Global Optim.* 11: 341–359. https://doi.org/10.1023/A:1008202821328.

Tran, A., J. Sun, J. M. Furlan, K. V. Pagalthivarthi, R. J. Visintainer, and Y. Wang. 2019. "pbo-2gp-3b: A batch parallel known/unknown constrained Bayesian optimization with feasibility classification and its applications in computational fluid dynamics." *Comput. Methods Appl. Mech. Eng.* 347 (Apr): 827–852. https://doi.org/10.1016/j.cma.2018.12.033.

Venturelli, G., and E. Benini. 2016. "Kriging-assisted design optimization of S-shape supersonic compressor cascades." *Aerosp. Sci. Technol.* 58 (Nov): 275–297. https://doi.org/10.1016/j.ast.2016.08.021.

Verstraete, T., F. Coletti, J. Bulle, T. Vanderwielen, and T. Arts. 2013. "Optimization of a U-bend for minimal pressure loss in internal cooling channels. Part 1: Numerical method." *J. Turbomach.* 135 (5): 1–10. https://doi.org/10.1115/1.4023030.

Verstraete, T., and J. Li. 2013. "Multi-objective optimization of a u-bend for minimal pressure loss and maximal heat transfer performance in internal cooling channels." In *Proc., ASME Turbo Expo 2013: Turbine Technical Conf. and Exposition*. San Antonio: ASME.

Yang, K., M. Emmerich, A. Deutz, and C. M. Fonseca. 2017. "Computing 3-D expected hypervolume improvement and related integrals in asymptotically optimal time." In *Proc., Int. Conf. on Evolutionary Multi-Criterion Optimization*, 685–700. New York: Springer.

Zerbinati, A., J.-A. Désidéri, and R. Duvigneau. 2012. *Application of metamodel-assisted multiple-gradient descent algorithm (MGDA) to air-cooling duct shape optimization*. Vienna, Austria: European Congress on Computational Methods in Applied Sciences and Engineering.